buildings

MDPI

Article

Experimental-Numerical Analysis of the Effect of Bar Diameter on Bond in Pull-Out Test

Marcin Burdziński * and Maciej Niedostatkiewicz

Department of Engineering Structures, Faculty of Civil and Environmental Engineering, Gdańsk University of Technology, 11/12 Gabriela Narutowicza Street, 80-233 Gdańsk, Poland
* Correspondence: marcin.burdzinski@pg.edu.pl

Abstract: Bar diameter is one of the basic factors affecting bond behavior, which is still of interest due to opposing opinions regarding its effect on bond behavior in the pull-out test. This paper presents an experimental and numerical bond analysis of ribbed reinforcing bar in concrete. The aim was to experimentally evaluate the effect of bar diameter on the bond behavior in the pull-out test and to perform numerical simulations of the conducted experiments in ABAQUS to verify their convergence to the obtained experimental results. The experiments used concrete of C35/45 grade and B500SP reinforcing steel bars of three diameters: 10, 12, and 16 mm. FEA simulations employed the Concrete Damaged Plasticity (CDP) material model and the Contact Cohesive Behavior (CCB) method to model the concrete–bar interface. The study shows that bar diameter significantly affects the bond, both on the bond stress–slip relationship and the type of bond failure, as well as on the bond strength. FEA simulations correctly reflected the bond behavior observed in the specimens. The analytical models presented estimates that were too conservative regarding the maximum bond stress relative to the experimental results.

Keywords: bond; concrete; FEM; pull-out test; ribbed steel reinforcing bar

check for updates

Citation: Burdziński, M.; Niedostatkiewicz, M. Experimental-Numerical Analysis of the Effect of Bar Diameter on Bond in Pull-Out Test. *Buildings* **2022**, *12*, 1392. https://doi.org/10.3390/buildings12091392

Academic Editors: Jia-Bao Yan and Francisco López Almansa

Received: 23 June 2022
Accepted: 26 August 2022
Published: 5 September 2022

Publisher's Note: MDPI stays neutral with regard to jurisdictional claims in published maps and institutional affiliations.

Copyright: © 2022 by the authors. Licensee MDPI, Basel, Switzerland. This article is an open access article distributed under the terms and conditions of the Creative Commons Attribution (CC BY) license (https://creativecommons.org/licenses/by/4.0/).

1. Introduction

Concrete is one of the most commonly used materials in construction. It is characterized by low tensile strength to compressive strength. Therefore, reinforcing bars are used in structural elements with tension zones. The interaction of concrete and bars allows forces to be transferred from the reinforcement to the surrounding concrete. This cooperation is known as bond. Nowadays, ribbed steel reinforcing bars are widely employed in engineering practice, which owe their high bond to concrete mainly to the ribs. According to [1], about 80% of the bond is due to the mechanical interlocking of the bar in the concrete, while the remaining 20% comes from the action of adhesion and friction. The force acting on the bar induces two forces around the rib: a pressure force (F_P) perpendicular to the rib surface and a friction force (F_F) parallel to the rib surface. The consequent resultant force (F_R) can then be decomposed into two components: a horizontal component (F_b) that transfers forces from the bar to the concrete and causes compression of the concrete between the ribs, and a vertical component (F_s) responsible for splitting the concrete (Figure 1).

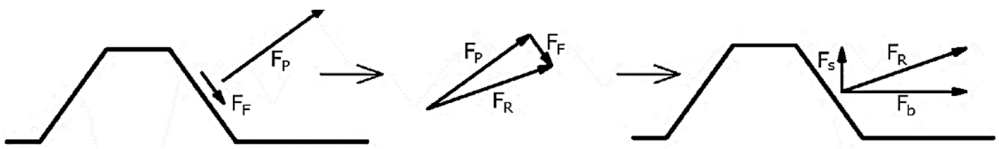

Figure 1. Forces on the bar rib (description in text).

The fundamental quantities of bond analysis are the bond stress (τ_b) and slip (s), which is the relative displacement between the concrete and the bar. Most often, one of the basic

results of bond analysis is the bond stress–slip curve $\tau_b(s)$. Rehm proposed that this curve is a fundamental law for bond, like the stress–strain curves for concrete or steel [2]. The shape of the curve indicates the type of bond failure. There are two types of bond failure: pull-out failure (POF) and splitting failure (SF) [3,4]. An example of $\tau_b(s)$ curves depending on the type of failure is shown in Figure 2.

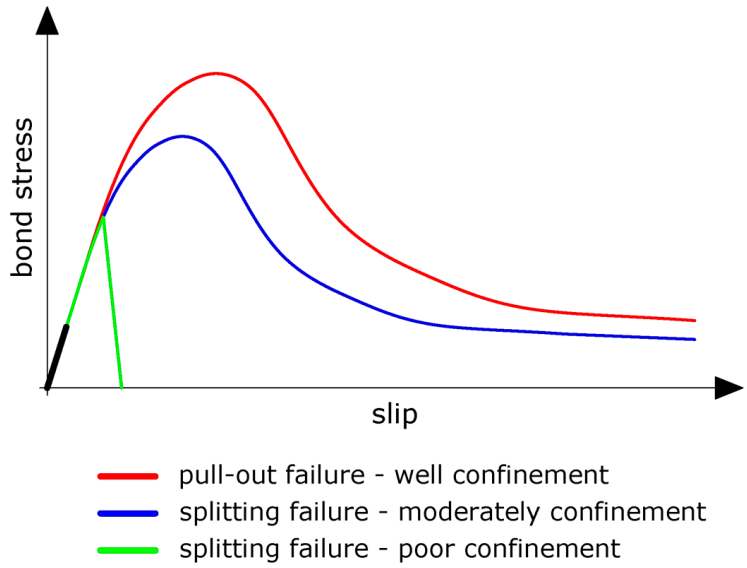

Figure 2. Example of $\tau_b(s)$ curves corresponding to type of bond failures.

The red curve in Figure 2 shows an example of the $\tau_b(s)$ relationship for pull-out failure. This situation occurs when the bar in the concrete is well confined. Then, the failure is caused by the horizontal component of the bond force. The initial, linear part of the graph (black section) corresponds to the range of adhesion action. As the slip increases, microcracks are formed, which are manifested by the nonlinearity of the $\tau_b(s)$ curve until the maximum value of the bond stress, called bond strength ($\tau_{b,max}$), is reached. Once the peak is exceeded, shearing of the concrete between the bar ribs takes place. The final stage is the friction at the concrete–concrete interface, i.e., the meeting of the concrete between the ribs and the concrete surrounding the bar, which results in stabilization of the curve. The other two curves in Figure 2 represent the bond stress–slip relationship for the splitting failure. In this situation, the bar confinement is insufficient to achieve the stress $\tau_{b,max}$. Beyond the linear range, the increasing slip induces radial and tangential stresses in the concrete due to the vertical component of the bond force, causing damage. This leads to the complete failure of the bond (green curve) when the bar is poorly confined in the concrete, or to a significant decrease in bond stresses, followed by a residual ability of the concrete and bar to cooperate when the confinement is moderate (blue curve).

One of the most commonly performed bond experiments is the pull-out test (POT). The purpose of the POT is to evaluate the effect of selected factors on the bond. The main test results are the $\tau_b(s)$ relationship and the maximum bond stress. This test has been performed since the 1940s. [5,6]. Currently, it is mostly used to analyze the influence of innovative materials on bond behavior (new generation concretes, non-metallic reinforcement, etc.) [7–10], as well as to evaluate the influence of accidental factors affecting the cooperation of the concrete and the bar [11–14]. The main disadvantages of the POT include lack of representation of the tensile zone of the RC members (the bar is in tension, while the concrete is in compression), slip-dependent bond function (bond stress is the same in each section), unprecedented in reinforced concrete confinement of the bar, leading to pull-out failure. The disadvantages above prevent the direct use of POT results in actual RC members [15].

Bond is affected by many factors. Among the most important of these are the concrete strength (compressive/tensile/shear strength), as well as those related to the bar

confinement in the concrete, which consists of the thickness of the bar cover, the presence of transverse reinforcement or the presence of external compressive/tensile stresses [16], and the embedded length. The geometry of the rebar also has a significant effect on the bond. Besides the relative rib area (f_R), the bar diameter bar is also important, as it is used in many issues related to the interaction of concrete and reinforcement, including in determining the bond strength needed to determine development length and splice length in Eurocode 2 [17] and fib Model Code 2010 [4]. In the standard [18], the bar diameter determines the parameters related to the geometry of its ribbing. The same standard [18] includes a procedure for conducting a pull-out test (based on the recommendations of RILEM [19]), which introduces representative diameters (d_b) for each of four bar-size groups. These groups are presented in Table 1.

Table 1. Series of bar diameters for pull-out test acc. [18].

Series Name	Bar	
	Range of Diameters [mm]	**Representative Diameter [mm]**
Small diameters	$d_b \leq 10$	8
Medium diameters	$10 < d_b \leq 20$	16
Large diameters	$20 < d_b \leq 32$	32
Very large diameters	$32 < d_b \leq 50$	Each size should be tested

Based on Table 1, it can be concluded that, for example, for the group of medium diameters, it is sufficient to conduct the test only for a diameter of 16 mm and assume that the results obtained will correspond to the bond behavior for the other diameters in this group. In pull-out tests, the bond length usually depends on the bar diameter. Most often, this length does not exceed five times the bar diameter ($l_b = 5d_b$). These samples are known as short specimens, which make it possible to assume that the bond stresses along the bond length have the same value [20–23].

In the literature, one can find papers in which the influence of the bar diameter on the bond behavior was investigated. However, there is no shortage of controversy, because in the work [24], it was found that increases of the diameter of the bar increase its bond, while in the publication [25], it was noted that, with an increase of the diameter of the ribbed bar, its bond decreases due to the lack of linearity between the increase of the relative rib area to the diameter. In addition, there is also the issue of the difference in the cooperation with concrete of thin [26] and large-diameter bars [27]. The difficulties in comparing test results due to differences in the conduct of the POT regarding test pieces (bond length, dimensions of concrete block) or additional factors affecting bond (concrete strength, material of rebar) are also worth keeping in mind. Taking all of this into account, it is difficult to say unequivocally how bar diameter affects bond behavior in the pull-out test.

Performing a numerical simulation of a pull-out test allows for a reliable representation corresponding to the actual course of the study [28,29], and allows for obtaining and observing results that cannot be obtained through experimentation (e.g., stress distribution in concrete). Computer programs based on the Finite Element Method (FEM) make analyses available using advanced material models and efficient ways to model the concrete and bar interaction, thereby allowing convergence with experimental results. There are two methods for POT simulation. The first method uses the actual shape of the reinforcement, that is, it models a ribbed bar. Then the bond properties related only to friction and adhesion are determined, since the mechanical interlocking phenomenon is due to the geometry of the bar [30,31]. The second method involves the modeling of a specimen with a plain bar, connected to the concrete by elements with specific properties to simulate the bond [32,33]. Then, it is necessary to use a bond model describing the relation $\tau_b(s)$. In this paper, the second method is employed for numerical simulation of the pull-out test.

This paper covers the scope of the experimental and numerical analysis of bond. The experimental analysis consisted of pull-out tests to evaluate the effect of diameter on the

bond behavior of steel ribbed bars in concrete under monotonic loading in this test. The test pieces were made without additional confinement and from typical materials that are most commonly found in construction practice today, so the only variable parameters of the test were the bar diameters, which were 10, 12, and 16 mm. On the other hand, the numerical analysis was intended to reflect the performance of the experimental specimens subjected to the pull-out test in terms of the adopted material models of concrete and steel, as well as to evaluate the assumed modeling method of the concrete-bar interface and bond behavior from the obtained empirical results. The investigation presented in the paper is a part of a broad research plan devoted to a comprehensive experimental-numerical bond analysis of specimens at various levels of observation of the concrete–rebar interaction [34]. The influence of basic factors affecting bond, such as the bar confinement in the concrete and the stress state of the specimen, will be analyzed, employing a pull-out test at different bond lengths and a beam test. The research plan aims, among other things, to develop a method for using the results of the pull-out test on short specimens in practical engineering applications affected by bond.

2. Materials and Methods

2.1. Concrete

Plain concrete grade C35/45 according to the standard [35] was adopted for the study. The following were used in the concrete mix: 0–2 mm fine aggregate, 2–8 and 8–16 mm coarse aggregate, Portland cement of strength class 42.5 MPa (CEM I 42.5R), meeting the requirements of the standard [36], and water. In addition, a superplasticizer was used to obtain the consistency of the concrete mix for convenient concreting of the specimens. After a trial series of concrete batches, the concrete mix composition shown in Table 2 was determined experimentally.

Table 2. Concrete mix composition.

Cement	Water	W/C Ratio	Fine Aggregate 0–2 mm	Coarse Aggregate 2–8 mm	Coarse Aggregate 8–16 mm	Super-Plasticizer
[kg/m^3]	[kg/m^3]	[–]	[kg/m^3]	[kg/m^3]	[kg/m^3]	[kg/m^3]
340	175	0.51	770	560	560	5.25

For each concrete batch intended for the POT test pieces, additional specimens were made to assess selected concrete parameters: cubes of 150 × 150 × 150 mm and cylinders of 150 mm diameter and 300 mm height. The concrete compressive strength (f_c) was determined on three cubes and three cylinders according to standard [37]. The concrete tensile strength by splitting (f_{ct}) was specified on three cubes according to standard [38]. The secant modulus of elasticity of concrete ($E_{c,s}$) was tested according to standard [39] by means of Method B. Six cylinders were used for this purpose: three for testing the modulus and three as companion specimens to define the upper-stress limit during the test. The resulting modulus of elasticity values were treated as a mean value of the modulus of elasticity (E_{cm}). In addition, the consistency of fresh concrete was also determined in accordance with the standard [40]. The tests of the aforementioned strength parameters were carried out for each concrete batch 28 days after the specimens were made. Based on these, the concrete parameters shown in Table 3 were defined. It was concluded that the concrete meets the requirements of grade C35/45, according to the standard [35].

Table 3. Test results of selected concrete parameters.

Concrete Consistency	Mean Value of Concrete Compressive Strength f_{cm}	Characteristic Compressive Cylinder Strength f_{ck}	Characteristic Compressive Cube Strength $f_{ck,cube}$	Mean Value of Concrete Tensile Strength f_{ctm}	Mean Value of Modulus of Elasticity E_{cm}
[-]	[MPa]	[MPa]	[MPa]	[MPa]	[GPa]
S3	43.47	38.89	47.62	3.10	33.62

2.2. Reinforcing Steel

Ribbed steel reinforcing bars with diameters of 10, 12, and 16 mm were accepted for testing. Bars were made of steel grade B500SP, which is often used in engineering practice in Poland. Reinforcing steel B500SP is steel with increased ductility (class C according to the standard [17]), which means that the ratio of characteristic strength values (f_{uk}) to the yield strength of reinforcing steel (f_{yk}) is in the range from 1.15 to 1.35, and characteristic strain corresponding to the steel strength (ε_{uk}) is no less than 7.5%. The value of f_{yk} for B500SP steel is in the range from 500 to 625 MPa. The requirements for the ribs and details of their geometry are given in Figure 3 and Table 4, according to the standard [41].

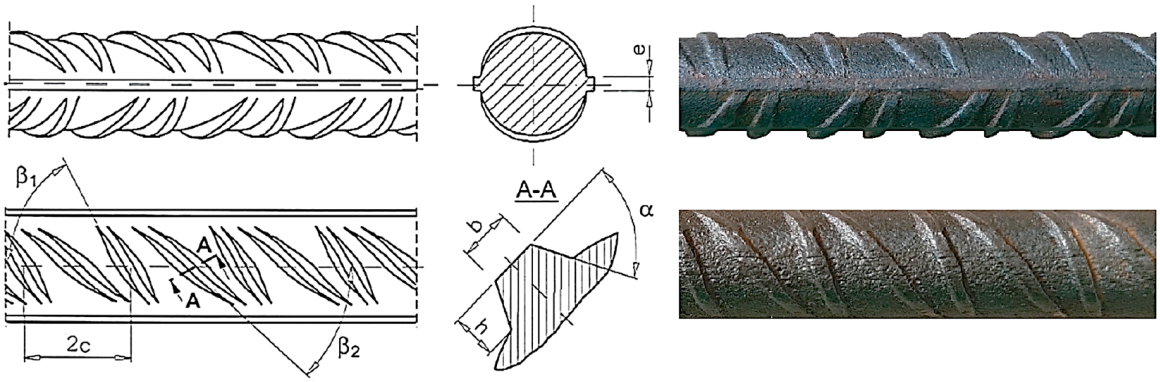

Figure 3. Parameters of deformed steel reinforcing bar B500SP [41] and its actual appearance.

Table 4. Properties of deformed steel reinforcing bars B500SP [41].

Parameter	Symbol	Unit	Minimum/limit
relative rib area	f_R	[-]	0.052 for $d_b = 10$ mm 0.056 for $d_b = 12, 16$ mm
flank inclination	α	[deg]	$\geq$45
pitch angle 1	β_1	[deg]	35 ÷ 75
pitch angle 2	β_2	[deg]	35 ÷ 75
distance	2c	[mm]	0.4d ÷ 1.2d
width	b	[mm]	N/A
height	h	[mm]	0.03d ÷ 0.15d
longitudinal bar width	e	[mm]	N/A
longitudinal bar height	h_1	[mm]	$\leq$0.15d

The yield strength (f_y), ultimate strength (f_u), ductility (k), and modulus of elasticity (E_s) were assessed for the described bars. The specimens were 400 mm in length. The elongation of the bar was measured using an extensometer at a measuring length of 50 mm. Three bars for each diameter were tested according to the standard [42]. The results of the rebar testing are shown in Table 5. Based on the results, it was found that the strength parameters meet the requirements for B500SP steel.

Table 5. Test results of selected strength parameters of reinforcing steel.

Bar Diameter d	Characteristic Yield Strength of Reinforcing Steel f_{yk}	Characteristic Strength of Reinforcing Steel f_{uk}	Ductility of Reinforcing Steel k	Characteristic Strain at Maximum Force ε_{uk}	Modulus of Elasticity of Reinforcing Steel E_s
[mm]	[MPa]	[MPa]	[-]	[%]	[GPa]
10	548	660	1.20	8.4	210
12	556	656	1.18	8.0	209
16	554	652	1.18	8.1	214

2.3. Experimental Analysis

The pull-out test was employed for an experimental analysis of bond. This test involves pulling a rebar anchored in a concrete block, and measuring the pull-out force (F) and the corresponding slip (s) at the same time. The bar diameter was the variable parameter of the experiment. Three diameters were considered: 10, 12, and 16 mm. Three series of POTs, one for each diameter, were performed. The series consisted of six specimens. Concrete and reinforcing steel were used for the test pieces, the parameters of which are described and listed above in Tables 2–5.

The specimens consisted of a concrete cubic block with a side length of 160 mm, which is ten times the diameter of the largest bar, and an anchored bar over a bond length equal to five times the bar diameter. The adoption of such a block size was aimed at observing the effect of bar confinement on the type of bond failure. A plastic tube with an outer diameter of 30 mm was placed on the unbonded part of the bar. To ensure the constant position of the bar in the block during concreting and compaction of the fresh concrete, the free space in the tube was filled with foam sealant. A rubber plug placed at the end of the tube filled with foam sealant to prevent the undesirable flow of concrete into its interior, therefore, the length l_b was not increased. The described method of securing the unbonded part of the bar was developed based on our own idea, which was verified during the POT pre-series. The concreting direction was perpendicular to the bar axis. An aluminum channel was glued to the side surface of the concrete block, upon which, the arm of an extensometer measuring slip rested, thus allowing for the measurement of the displacement of the concrete block in relation to the bar. Figure 4 shows a POT specimen. Details of the POT series are shown in Table 6.

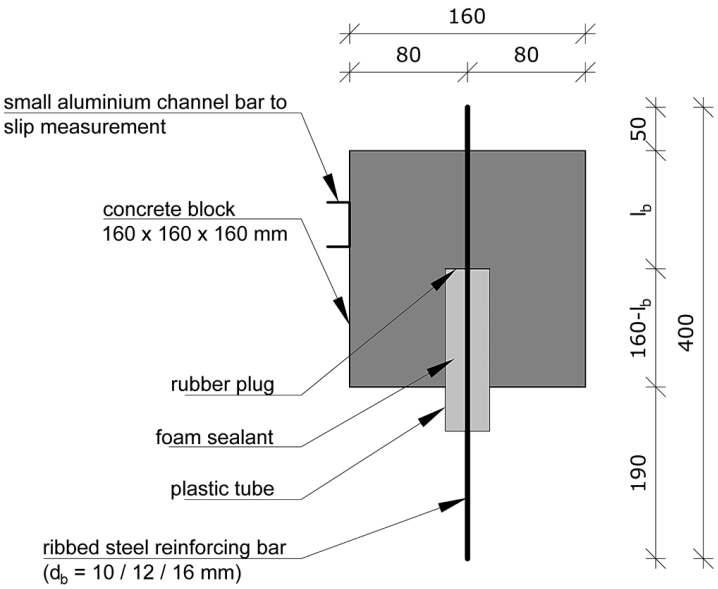

Figure 4. Pull-out test specimen.

Table 6. Pull-out test series details.

Series Name	Bar Diameter d_b	Bond Length l_b	Bar Cover c	c/d_b Ratio	Number of Specimens in a Series
[-]	[mm]	[mm]	[mm]	[-]	[-]
POT-10	10	50	75	7.5	6
POT-12	12	60	74	6.2	6
POT-16	16	80	72	4.5	6

The test pieces were placed in a specially designed steel cage, mounted in a testing machine (Zwick Roell Z400). A steel bar welded to the top plate of the cage was clamped in the upper, movable part of the machine. The rebar of the specimen was clamped in the lower, stationary part of the machine. The plates were connected by a 16 mm diameter bar ending in threads and nuts with washers. Under the specimen, a pad was placed to minimize friction between the concrete block and the steel plate, which would cause additional confinement of the concrete and the bar. The pad consisted of two layers: a bottom layer of 3 mm thick rubber and an upper layer of 6 mm thick polyethylene sheet. A schematic and actual view of the test stand is shown in Figure 5.

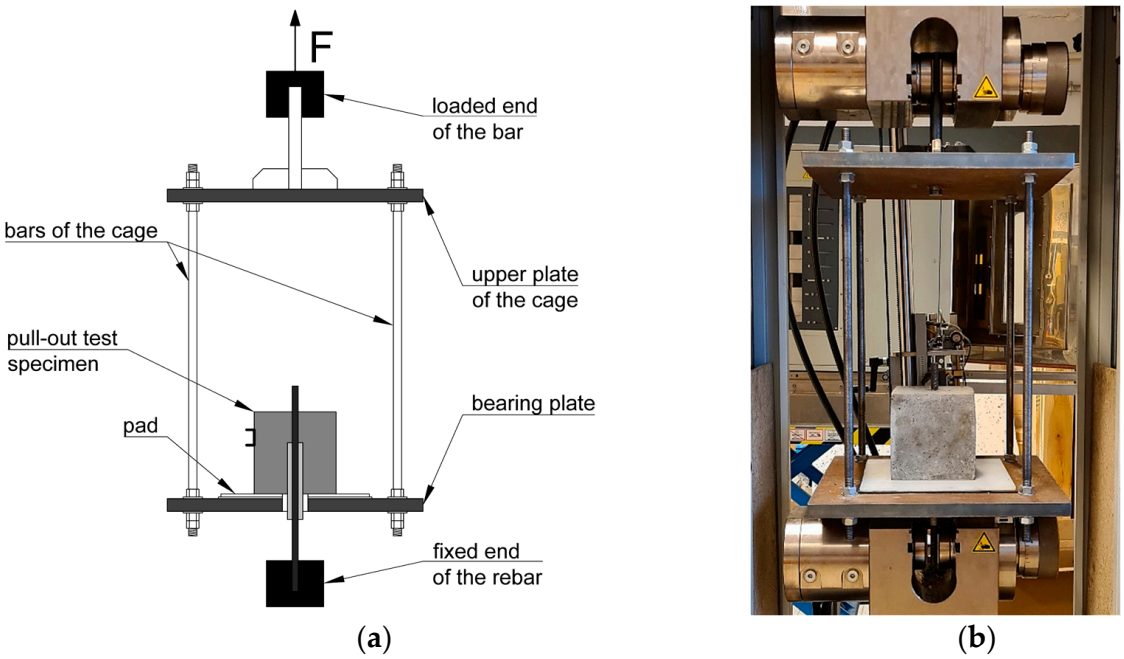

Figure 5. Test stand for the pull-out test: (**a**) Schematic view with details; (**b**) Actual view.

The load was applied to the specimens by the lower cage plate (the cage plates were thick enough to be assumed non-susceptible) by a monotonic displacement increment at a rate of 1 mm/min, to ensure static loading of the test piece. Controlling the load by displacement made it possible to observe bond behavior after the maximum value of bond stress was reached, which would not have been possible if the load was controlled by a constant increment of force. The test was carried out up to a maximum slip value of 30 mm, or until the force dropped below 1% of the maximum force achieved in the test. All experiments were performed 28 days after the specimens were made. The result of the test was a curve of the local bond stress–slip relationship $\tau_b(s)$. The bond stress τ_b was determined according to the formula:

$$\tau_b = \frac{F}{\pi \cdot d_b \cdot l_b}. \quad (1)$$

The measured slip value s was reduced by the elongation of the portion of the bar that was not anchored in concrete (l_i), determining the actual slip value at the i-th step according to the formula:

$$l_i = \frac{(F_i - F_0) \cdot (l + \Delta l_{i-1})}{E_s \cdot A_s}, \quad (2)$$

where: F_i—pull-out force of the bar in the i-th step; F_0—initial pull-out force; l—initial length of the bar not anchored in concrete; Δl_{i-1}—increment of the length of the unanchored part of the bar in step $i - 1$; E_s—elastic modulus of the reinforcing steel; A_s—cross-sectional area of the bar. Formula (2) is true under the assumption that the reinforcing steel operates in the linear elastic range.

2.4. Numerical Analysis

Numerical analysis of the pull-out test was performed in the ABAQUS program. To carry out the FEM simulation, it was necessary to define material models of concrete and reinforcing steel reflecting their actual behavior in the experiments. In addition, it was also necessary to choose a method. The bond properties associated with the chosen method had to be determined, as well.

The elastic range and plastic range were defined in the concrete material model using the Concrete Damaged Plasticity (CDP) model. A dilatation angle of 35° and a viscosity parameter of 0.008 were used to describe the complex stress state, while default values were used for the other parameters of the CDP model (Table 7). On the other hand, the stress–strain relationship for compression and stress–crack opening for tension were employed to describe the behavior of concrete in the uniaxial state (Figure 6), as well as parameters corresponding to concrete grade C35 from MC2010 [4] (Table 8). The exception was the fracture energy (G_F), the value of which was assumed according to the ABAQUS documentation [43]. In addition, the stress–strain relationship for compression was set to be linear, up to a stress value equal to 40% of the concrete compressive strength, which determined the obtaining of a new value for the secant modulus of concrete (E_{cm}).

Table 7. Concrete Damaged Plasticity model parameters.

Dilatation Angle	Eccentricity	fb0/fc0	K	Viscosity Parameter
[deg]	[-]	[-]	[-]	[-]
35	0.1	1.16	0.667	0.008

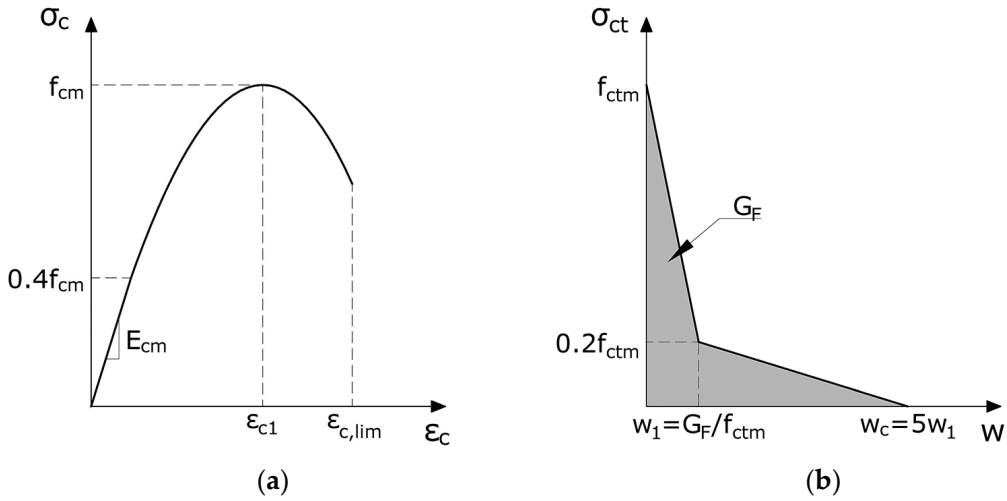

Figure 6. Concrete acc. MC2010 [4]: (**a**) Stress–strain relationship in compression; (**b**) Stress–crack opening in tension.

Table 8. Concrete parameters in numerical simulations.

Characteristic Compressive Cylinder Strength of Concrete f_{ck}	Characteristic Compressive Cube Strength of Concrete $f_{ck,cube}$	Mean Value of Concrete Compressive Strength f_{cm}	Mean Value of Concrete Tensile Strength f_{ctm}	Poisson's Ratio ν_c	Tangent Modulus of Elasticity E_{ci}
[MPa] 35	[MPa] 45	[MPa] 43	[MPa] 3.2	[-] 0.2	[GPa] 35.0
Tangent Modulus of Elasticity (frome 0 to f_{cm}) E_{c1}	**Tangent Modulus of Elasticity (frome 0 to 0.4f_{cm}) E_{cm}**		**Strain Corresponding to f_{cm} ε_{c1}**	**Limit Strain $\varepsilon_{c,lim}$**	**Fracture Energy G_F**
[GPa] 18.2	[GPa] 32.2		[‰] −2.3	[‰] −3.5	[N/mm] 0.120

Parameters of the elastic range were defined in the material model of reinforcing steel. The stress–strain relationship was assumed to be linear. The value of the modulus of elasticity was taken depending on the diameter of the bar, according to Table 5.

The bond behavior in the pull-out test is described by the local bond stress–slip relationship. The numerical POT simulations employ the bond model represented in MC2010 [4] (Figure 7). For monotonic loading, bond stress values are calculated according to Equations (3)–(6). Table 9 defines the characteristic points of the model. Justification of the rules and assumptions of the presented model is given in ref. [16].

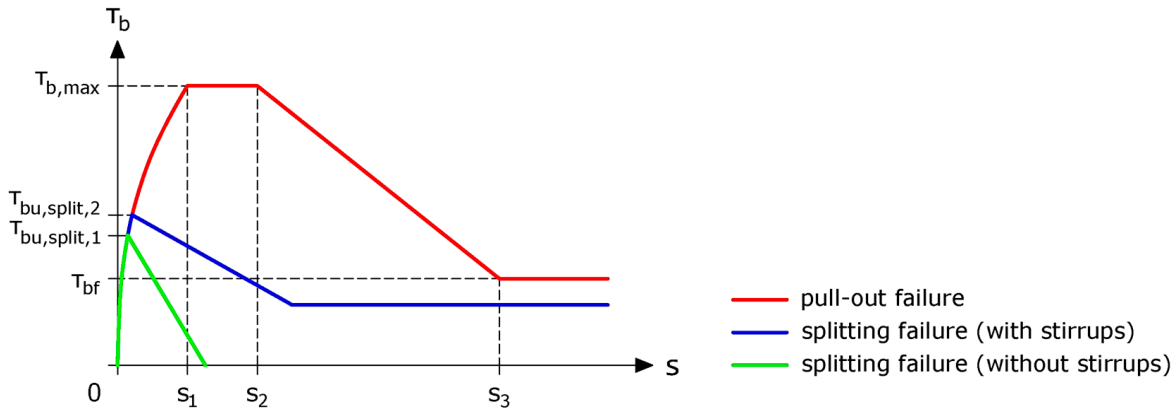

Figure 7. Analytical bond stress-slip relationship for monotonic loads acc. MC2010 [4].

For $0 \leq s \leq s_1$:

$$\tau_b(s) = \tau_{b,max} \cdot \left(\frac{s}{s_1}\right)^{\alpha} \tag{3}$$

For $s_1 < s \leq s_2$:

$$\tau_b(s) = \tau_{b,max} \tag{4}$$

For $s_1 < s \leq s_2$:

$$\tau_b(s) = \tau_{b,max} - (\tau_{b,max} - \tau_{bf}) \cdot \frac{s - s_2}{s_3 - s_2} \tag{5}$$

For $s_3 < s$:

$$\tau_b(s) = \tau_{bf} \tag{6}$$

The Contact Cohesive Behavior (CCB) method available in ABAQUS was employed to model the concrete–bar interface. This method allows for an efficient representation of the bond behavior considering the bond stress–slip law. With CCB, it is possible to simulate

the linear-elastic range of the $\tau_b(s)$ relationship, as well as the initiation and evolution of damage using the traction-separation law. The linear-elastic traction-separation law for the uncoupled stiffness option is expressed by the equation:

$$\begin{Bmatrix} t_n \\ t_s \\ t_t \end{Bmatrix} = \begin{bmatrix} K_{nn} & 0 & 0 \\ 0 & K_{ss} & 0 \\ 0 & 0 & K_{tt} \end{bmatrix} \begin{Bmatrix} \delta_n \\ \delta_s \\ \delta_t \end{Bmatrix}. \quad (7)$$

The meaning of the subscripts (n, s, t) from Equation (7) for the directional designation in the CCB was shown in Figure 8.

Table 9. Definition of characteristic points of the bond model acc. MC2010 [4] for deformed bars.

	Pull-Out		**Splitting**			
			$\varepsilon_s < \varepsilon_{s,y}$			
	Good Bond Conditions	**Other Bond Conditions**	**Good Bond Conditions**		**Other Bond Conditions**	
			without Stirrups	**with Stirrups**	**without Stirrups**	**with Stirrups**
$\tau_{b,max}$	$2.5\sqrt{f_{cm}}$	$1.25\sqrt{f_{cm}}$	$2.5\sqrt{f_{cm}}$	$2.5\sqrt{f_{cm}}$	$1.25\sqrt{f_{cm}}$	$1.25\sqrt{f_{cm}}$
$\tau_{bu,split}$	N/A	N/A	$7.0\cdot\left(\frac{f_{cm}}{25}\right)^{0.25}$	$8.0\cdot\left(\frac{f_{cm}}{25}\right)^{0.25}$	$5.0\cdot\left(\frac{f_{cm}}{25}\right)^{0.25}$	$5.5\cdot\left(\frac{f_{cm}}{25}\right)^{0.25}$
s_1	1.0 mm	1.8 mm	$s(\tau_{bu,split})$	$s(\tau_{bu,split})$	$s(\tau_{bu,split})$	$s(\tau_{bu,split})$
s_2	2.0 mm	3.6 mm	s_1	s_1	s_1	s_1
s_3	c_{clear}*	c_{clear}*	$1.2s_1$	$0.5c_{clear}$*	$1.2s_1$	$0.5c_{clear}$*
α	0.4					
τ_{bf}	$0.4\tau_{b,max}$	$0.4\tau_{b,max}$	0	$0.4\tau_{b,max}$	0	$0.4\tau_{b,max}$

* c_{clear}—distance between adjacent ribs; $0 \leq \alpha \leq 1$—curve shape parameter (default: 0.4).

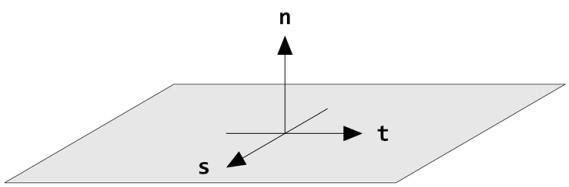

Figure 8. Directions interface for Contact Cohesive Behavior in ABAQUS.

For the pull-out test simulations, "Traction" is interpreted as bond stress, and "Separation" as slip, allowing the local bond model to be used directly in describing bond behavior. The stiffness K is equal to the stiffnesses K_{ss} and K_{tt}. It is determined as follows:

$$K = K_{ss} = K_{tt} = \frac{\tau_{b,lin}}{s_{lin}}, \quad (8)$$

where: $\tau_{b,lin}$—the limiting bond stress terminating the linear relationship $\tau_b(s)$, s_{lin}—the slip corresponding to the stress $\tau_{b,lin}$. According to Keuser et al. [44], the stiffness K_{nn} is determined by the formula:

$$K_{nn} = 100 \cdot K. \quad (9)$$

In addition to the definition of bond stiffness itself, it is also necessary to determine the parameters associated with its damage. The first parameter is the initiation of damage. In the simulations performed, the Maximum Stress criterion (MAXS) was used. When the criterion is met, the damage is initiated. The next stage is the development of damage. In the ABAQUS software for CCB, this is done through the Damage Evolution Law. The law describes the rate at which the cohesive stiffness is degraded. Degradation is considered by a scalar variable (D) representing the overall damage at the contact point. The variable D takes a value from 0 (no damage) to 1 (full damage). Thus, the D value increases as

the damage progress. In this situation, the form of Traction–Separation Law expresses the formula:

$$t = (1 - D)K\delta. \tag{10}$$

Damage Evolution controlled by displacement was adopted for simulations. The tabular method of the softening was employed. It was therefore necessary to determine the values of D and the corresponding inelastic slips (s_{in}). The value of the degradation variable, which is dependent on the slip value, can be calculated according to the formula:

$$D = 1 - \frac{\tau_b(s)}{K \cdot s}, \tag{11}$$

where: $\tau_b(s)$ is calculated according to Equations (3)–(6); K is determined from Equation (8). The slip s_{in} is obtained by subtracting the slip corresponding to the stress $\tau_{b.lin}$ from the total slip s:

$$s_{in} = s - s_{lin}. \tag{12}$$

An axisymmetric model was used for numerical simulations in ABAQUS. For the calculations, the ABAQUS Standard solver was employed. Both the concrete block and the rebar were discretized using 4-node bilinear axisymmetric quadrilateral (CAX4) finite elements. Three finite element sizes were adopted in the model: 1.0, 2.0 and 4.0 mm. Figure 9 shows the finite element mesh of the specimen for POT-12 series. For the other cases, the model differed only in bar diameter.

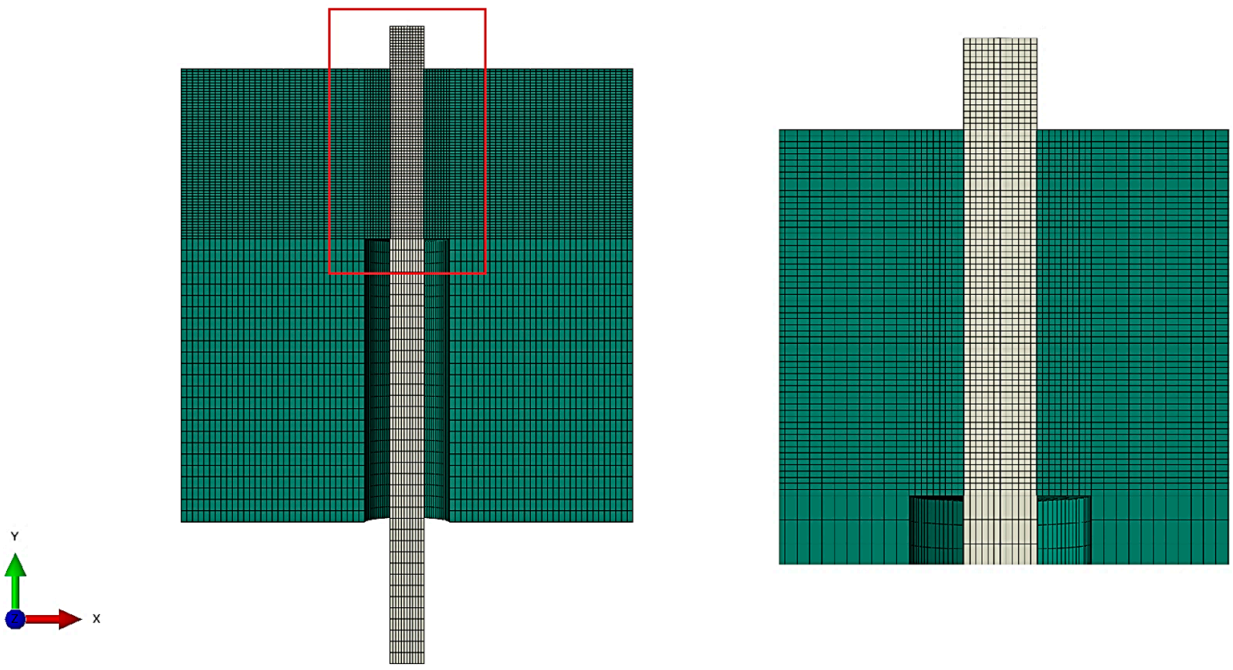

Figure 9. Finite element mesh for POT-12 specimen in ABAQUS.

3. Experimental Analysis–Results and Discussion

3.1. Local Bond Stress-Slip Relationship

Based on the series of pull-out tests, the curves of the local stress–slip relationship were created. Figures 10–12 show the course of representative $\tau_b(s)$ curves being the average of the results obtained from six specimens from the series together with the envelope.

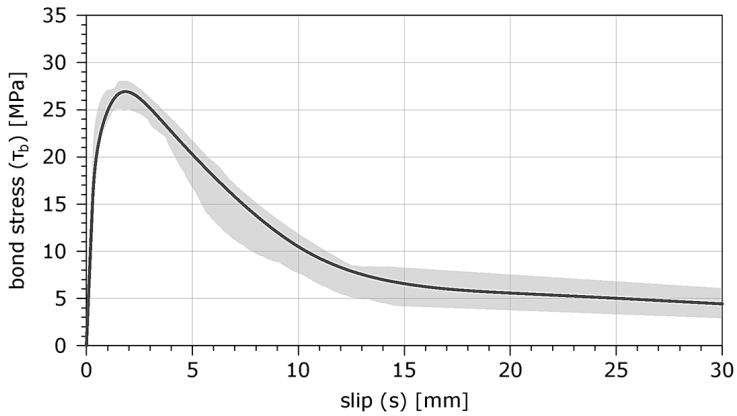

Figure 10. Bond stress–slip curve for POT-10 series (d_b= 10 mm).

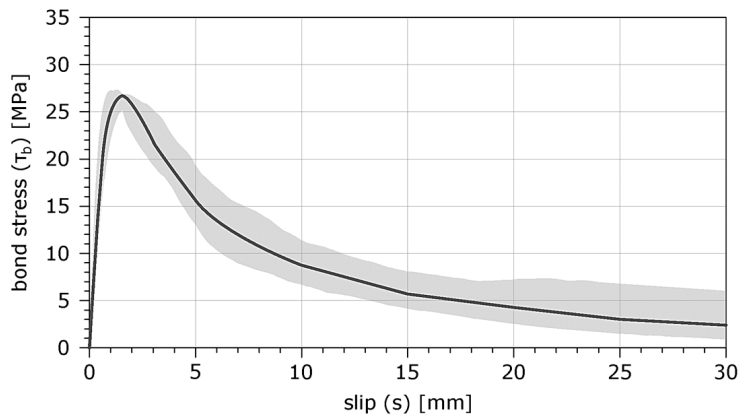

Figure 11. Bond stress–slip curve for POT-12 series (d_b= 12 mm).

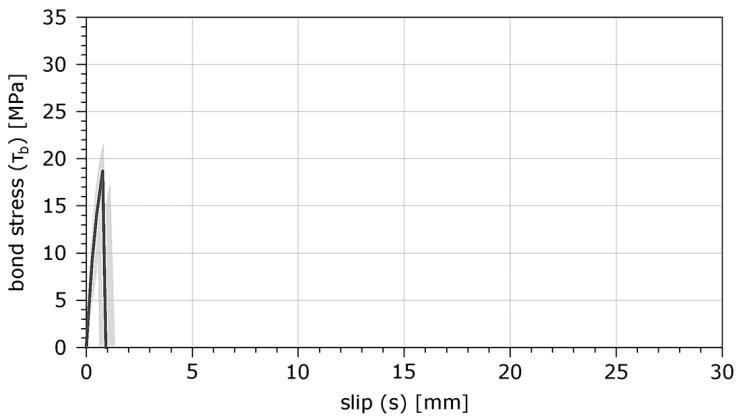

Figure 12. Bond stress–slip curve for POT-16 series (d_b= 16 mm).

The shape of the $\tau_b(s)$ curve for the POT-10 and POT-12 series (Figures 10 and 11) indicates that the specimens were damaged by pull-out, while the POT-16 series specimens (Figure 12) were damaged by splitting (cf. Figure 2). The use of different bar sizes and bond lengths dependent on bar diameter resulted in variable conditions of bar confinement in concrete, which led to different types of bond failure. According to MC2010 [4], pull-out failure occurs when the ratio of the concrete bar cover to the bar diameter is no less than five. As seen in Table 6, this condition was met by specimens of the POT-10 and POT-12 series, which proves the correctness of the aforementioned notation. However, it should be noted that this notation probably refers to the situation when the bond length is five times the bar diameter. A similar assumption was made in MC2010 [4] for the semi-empirical formula for the bond stress at splitting failure ($\tau_{bu,split}$). Examples of specimens after testing are shown in Figure 13.

(**a**) (**b**) (**c**)

Figure 13. Pull-out test specimens after testing: (**a**) POT-10; (**b**) POT-12; (**c**) POT-16.

Figure 14 shows representative $\tau_b(s)$ curves for the conducted POT series. The initial, linear-elastic range is almost identical for all shown curves, indicating similar bond stiffness. In the non-linear range before the peak, the first discrepancies in their course appeared, especially for the POT-16 series, whose specimens reached the maximum bond stress in this range.

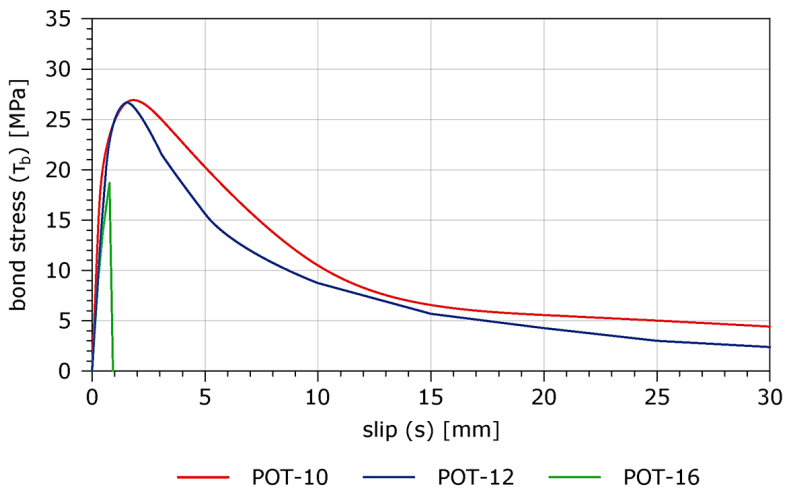

Figure 14. Comparison of representative curves obtained from pull-out tests.

For the POT-12 series, a faster degradation of post-peak bond stress is evident compared to the POT-10 series. This represents a faster degradation of bond stiffness due to the shearing-off of the concrete between the ribs. This is the result of greater bar confinement, owing to the thicker concrete cover. The smaller diameter affected the slower degradation of stiffness after the peak. This may also be influenced by the slightly different ribbing of the bar, which depends on the diameter. The $\tau_b(s)$ curves of the POT-10 and POT-12 series start to stabilize at a slip value of 15 mm, reaching residual bond stress (τ_{bf}), which is about 20% of the maximum bond stress.

3.2. Maximum Bond Stress

Table 10 shows the extreme and mean maximum bond stresses obtained from the experiments, which were determined according to Equation (1). In addition, standard deviations (σ) and coefficients of variation (CV) were given.

Table 10. Summary of maximum bond stresses.

Series Name	Maximum Bond Stress [MPa]			Standard Deviation σ [-]	Coefficient of Variation CV [%]
	MIN	MAX	MEAN		
POT-10	25.12	28.05	26.85	1.07	4.0
POT-12	25.22	27.32	26.69	0.77	2.9
POT-16	16.71	21.50	18.68	2.03	10.9

The differences between the extreme values for specimens of the POT-10 and POT-12 series are small, as evidenced by the low coefficient of variation—4.0 and 2.9%, respectively. The low variability is also evidenced by the envelopes of the results for the series shown in Figures 10 and 11. Such a small scatter in the results confirms the proper preparation of the test pieces, especially in terms of ensuring the assumed bond length. Larger scatter in the extreme maximum bond stresses occurred in the POT-16 series, as the CV for these specimens was 10.9%. This is an acceptable value, given the probabilistic nature of bond. The steeper slope of the green curve representing the POT-16 series in Figure 14 is relative to the other two. This is the effect of averaging results characterized by greater scatter. For the POT-16 series, the mean maximum bond stress is lower, and is about 70% of the mean stresses of the POT-10 and POT-12 series, which is due to a different type of bond failure.

The effect of bar diameter on the experimental results obtained is insignificant, as the difference between the mean strength values of the POT-10 and POT-12 series specimens was 0.16 MPa. The bond length, depending on the bar diameter, allowed the specimen to obtain almost identical maximum adhesion stresses for the pull-out failure. This is an important observation in terms of the division into groups of bars of different diameters made in the pull-out test procedure in the standard [18] (see Table 1). Thus, it can be assumed that, in the case of providing greater confinement of a 16 mm diameter bar in concrete (for example, through a larger size of the concrete block), the specimen would be damaged by pull-out, and the maximum bond stresses would be like those obtained for the POT-10 and POT-12 series. Similar values of the maximum bond stress in the POT for various diameters and bond lengths, depending on d_b, were observed in the papers [45,46].

3.3. Slip and Maximum Pull-Out Force

Table 11 shows the extreme and mean slips along with σ and CV and the pull-out forces corresponding to the maximum bond stresses.

Table 11. Summary of slips and forces corresponding to maximum bond stresses.

Series Name	Slip s [mm]			Standard Deviation σ [-]	Coefficient of Variation CV [%]	Maximum Pull-Out Force F_{max} [N]		
	MIN	MIN	MEAN			MIN	MAX	MEAN
POT-10	1.73	2.03	1.86	0.17	9.1	39,458	44,061	42,171
POT-12	1.15	1.65	1.52	0.31	20.4	57,046	61,796	60,379
POT-16	0.52	1.12	0.77	0.21	27.3	67,195	86,457	75,130

Larger mean slip s_{max} values were achieved in the POT-10 series specimens than in the POT-12 series. This was most likely thanks to better confinement of the bar by the concrete cover. For the POT-16 series, the mean slip value was about half as much, which was due to the splitting failure. As the bar diameter increased, the coefficient of variation increased, which did not exceed 30% for any series.

While the mean bond strengths for the POT-10 and POT-12 series were almost the same, the values of the pull-out forces (F_{max}) differed significantly. From the obtained

results, it can be seen that the larger the bar diameter, the higher the force required to pull the bar out of the concrete. This is an obvious conclusion, since the bond lengths were determined by the bar diameter (the larger the diameter, the greater the bond length). The determination of the bond stresses according to Equation (1) is based on the assumption that the pull-out force is uniformly distributed on the lateral bar surface. This allows qualitative comparison of bond for different bar diameters and bond lengths.

4. Numerical Analysis–Results and Discussion

4.1. Bond Parameters in Numerical Simulations

One method to define the bond behavior in numerical simulations of a pull-out test in ABAQUS using the CCB is to use a bond model that defines a local bond stress–slip relationship. For this purpose, the model described in MC2010 [4] was employed. Based on the relationship presented in Figures 10–12, it was considered that the curves for the POT-10 and POT-12 series are described by the curve corresponding to the pull-out failure, and for the POT-16 series by the curve corresponding to the splitting failure without stirrups (see Figure 7). "Good bond conditions" were assumed for all series. In Table 12, the values of the characteristic points of the bond stress–slip curves obtained from the experiments and from the MC2010 bond model were compared. The parameters from the experiments were adjusted to best match the bond model curve with the representative curves from the experiments.

Table 12. Summary of characteristic point values of the bond stress–slip curves.

	Experimental Results	**Bond Model acc. MC2010 [4]**	**Experimental Results**	**Bond Model acc. MC2010 [4]**
Series name	POT-10/POT-12		POT-16	
Type of bond failure	pull-out failure (POF)		splitting failure (SF)	
Bond conditions	good bond conditions		good bond conditions without stirrups	
$\tau_{b,max}$ **[MPa]**	26.85/26.69	16.41	26.85/26.69	16.41
$\tau_{bu,split}$ **[MPa]**	N/A	N/A	18.76	8.02
s_1 **[mm]**	1.00	1.00	0.49	0.17
s_2 **[mm]**	2.00	2.00	0.49	0.17
s_3 **[mm]**	9.00	6.00	0.65	0.20
α **[-]**	0.5	0.4	0.5	0.4
τ_{bf} **[MPa]**	5.36	6.57	0.00	0.00

By means of Equations (3)–(6), $\tau_b(s)$ curves were created using the characteristic point values given in Table 12, which are shown in Figure 15. FEM simulations were performed in the slip range from 0 to 15 mm.

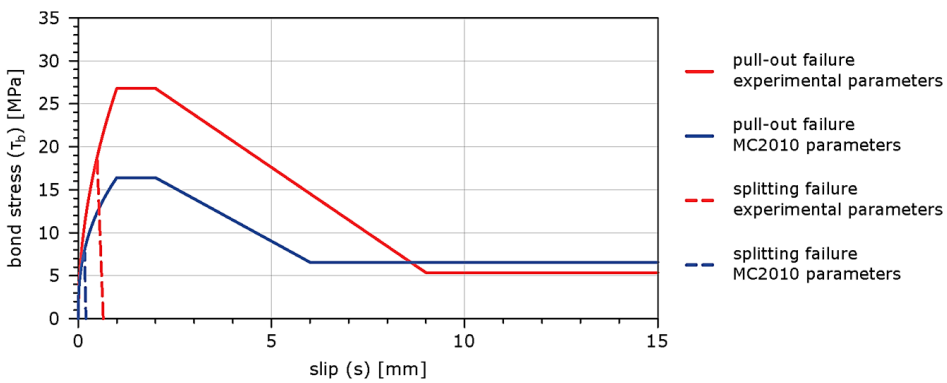

Figure 15. Bond model acc. MC2010 [4] for characteristic points obtained from experiments and from standard.

Many proposals of formulas for determining the maximum bond stresses have been described in the literature. Most of them consist of the product of the square root of the mean concrete compressive strength and a coefficient, which takes different forms depending on the approach used. In the formula proposed in MC2010 [4] for pull-out failure, the coefficient is a constant value. The same applies to the formula described by Harajli et al. [47]. In the Australian standard AS 3600 [48], the coefficient depends on the ratio of the bar cover thickness to the bar diameter, while in the formula presented by Orangun et al. [49], the coefficient additionally depends on the ratio of the bar diameter to the bond length. This formula was further developed by Darwin et al. [50], who also considered the effect of the ratio of maximum to minimum bar cover thickness. There are also proposals to determine the maximum bond stress for POF based on the product of the mean concrete compressive strength and a coefficient, which was proposed by Huang et al. [51]. In addition, MC2010 [4] also provides a separate formula for calculating the maximum stress τ_b for a splitting failure. Table 13 summarizes the aforementioned formulas for determining maximum bond stress along with the values, as well as the values obtained from experiments. In brackets, the percentages of maximum bond stress to experimental results were given.

Table 13. Parametric analysis of maximum bond stress.

Source	Equation (SI Units)	Series		
		POT-10	POT-12	POT-16
		[MPa]		
Experiments	N/A	26.85 (100%)	26.69 (100%)	18.76 (100%)
MC2010–POF [4]	$2.5\sqrt{f_{cm}}$	16.39 (61%)	16.39 (61%)	N/A
Harajli et al. [47]	$2.57\sqrt{f_{cm}}$	16.85 (63%)	16.85 (63%)	N/A
AS 3600 [48]	$0.265\left(\frac{c}{d_b}+0.5\right)\sqrt{f_{cm}}$	13.90 (52%)	11.58 (43%)	8.69 (46%)
Orangun et al. [49]	$0.08\left(1.2+3\frac{c}{d_b}+50\frac{d_b}{l_b}\right)\sqrt{f_{cm}}$	17.68 (66%)	15.58 (58%)	12.96 (69%)
Darwin et al. [50]	$0.08\left[\left(1.06+2.12\frac{c}{d_b}\right)\left(0.92+0.08\frac{c_{max}}{c_{min}}\right)+75\frac{d_b}{l_b}\right]\sqrt{f_{cm}}$	16.77 (62%)	15.28 (57%)	13.43 (72%)
Huang et al. [51]	$0.45f_{cm}$	19.35 (72%)	19.35 (72%)	N/A
MC2010–SF [4]	$7.0\left(\frac{f_{cm}}{25}\right)^{0.25}$	N/A	N/A	8.02 (43%)

The best agreement with the experimental results of the maximum bond stresses for the pull-out failure was obtained by the formula given by Huang et al. [51] (72%), and for splitting failure, by the formula proposed by Darwin et al. [50] (72%). In contrast, the least convergent results were obtained by the formula according to AS 3600 [48] for POF (52% and 43%), and according to MC2010 [4] for SF (43%). Comparing the curves $\tau_b(s)$ shown in Figure 15, one can see significant differences in their courses. Therefore, the use of curves described in the bond model in MC2010 [4] was determined to be the best approach, based on characteristic points specified from the experimental results.

In the definition of the cohesive surface in ABAQUS, the stiffness of the concrete–bar interface should also be defined. It was assumed that the linear relationship $\tau_b(s)$ occurs up to a value of 15% of the maximum bond stress ($\tau_{b,lin}$), which well reflects the range of adhesion action during the test. At the same time, the stress $\tau_{b,lin}$ initiates the bond stiffness degradation process. Using Equations (8) and (9), the bond stiffnesses shown in Table 14 were obtained.

Table 14. Bond stiffnesses for FEM simulation of pull-out tests.

K_{nn} [MPa/mm]	K_{ss} [MPa/mm]	K_{tt} [MPa/mm]
17,866.67	178.67	178.67

4.2. Comparative Analysis of Experimental and Numerical Results–POT-10 and POT-12 Series

Numerical simulations employed the same $\tau_b(s)$ curve for the POT-10 and POT-12 series corresponding to pull-out failure. After pre-simulations, the curves describing the bond behavior were calibrated to best match the experimental results. Figures 16 and 17 compare the curves obtained from experiments, FEM simulations, and bond model for POT-10 and POT-12, respectively.

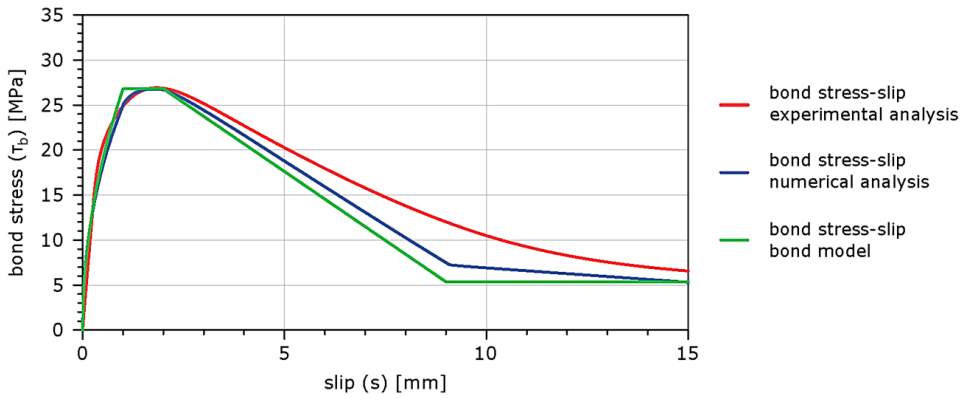

Figure 16. Comparison of bond stress–slip curves for the POT-10 series.

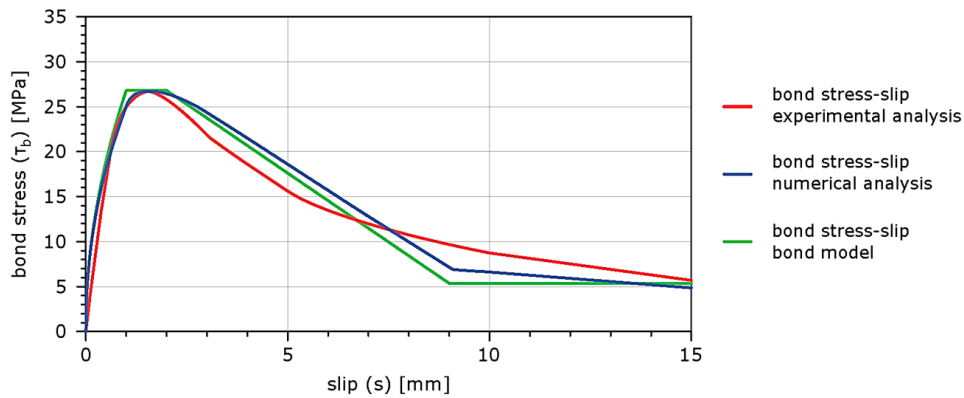

Figure 17. Comparison of bond stress–slip curves for the POT-12 series.

In the pre-peak and peak ranges, all three curves have a remarkably similar course. This proves that the parameters of the bond model and the parameters describing bond in ABAQUS were properly chosen. The differences in the curves start in the post-peak range, especially between the experimental and numerical curves. This is directly due to the use of a linear bond stress–slip relationship, which is an oversimplification of the $\tau_b(s)$ curve description proposed in MC2010 [4] for this range. For the range of residual bond stress, there are also noticeable discrepancies between the experimental and numerical results. Nevertheless, the overall course of the curves adequately describes the trend of the $\tau_b(s)$ curves.

4.3. Comparative Analysis of Experimental and Numerical Results–POT-16 Series

Numerical simulations employed $\tau_b(s)$ curve for the POT-16 series corresponding to splitting failure. Analogously to the POT-10 and POT-12 series, pre-simulations were performed to calibrate the model. Figure 18 summarizes the curves as for the previously described analyses.

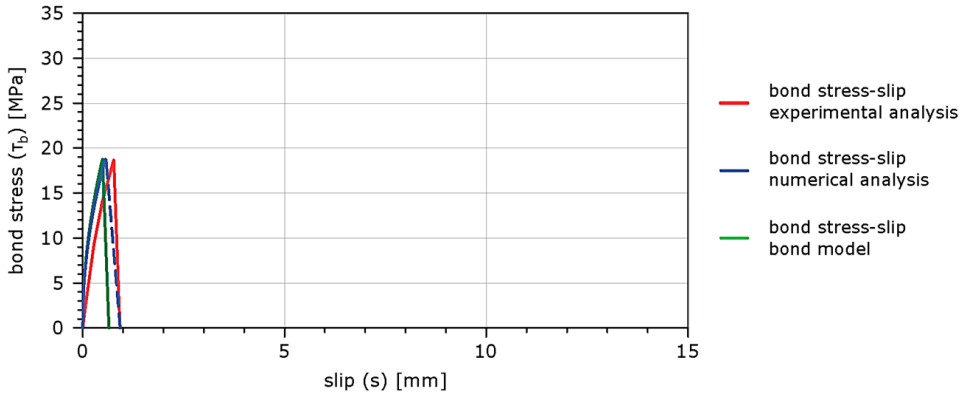

Figure 18. Comparison of bond stress-slip curves for the POT-16 series.

The numerical simulation of the POT-16 series was not completed due to convergence problems. The dashed line for the numerical curve is an extension of the curve where the calculations stopped. Based on Figure 18, there is good agreement between the numerical curve and the curve from the bond model in the pre-peak range. The experimental curve differs from the other two. This is because it is a curve averaging the results of the six specimens of the POT-16 series, which had the largest scatters (see Table 10).

Figures 19–21 show the maximum principal stresses corresponding to the maximum bond stresses.

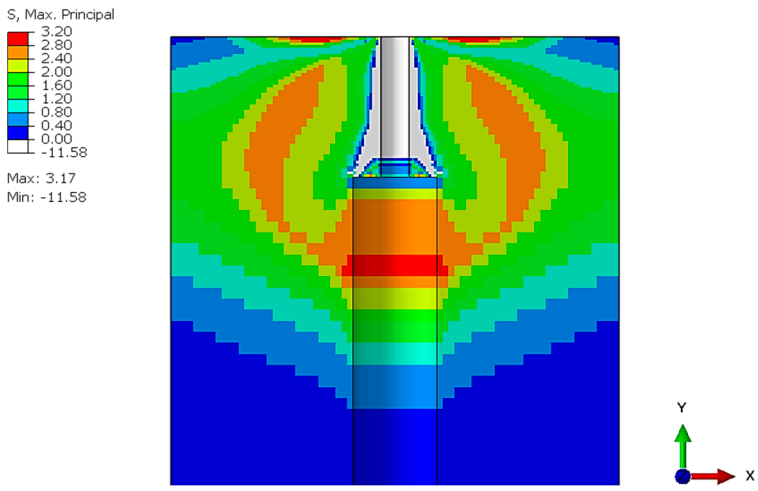

Figure 19. Map of maximum principal stresses for the POT-10 series.

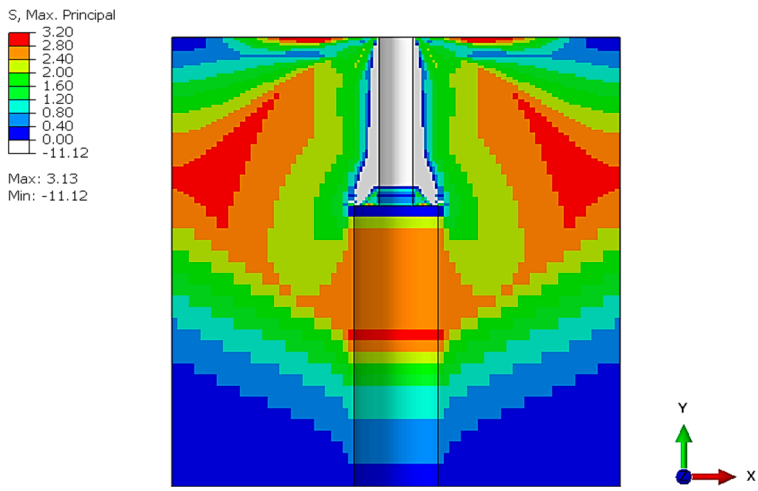

Figure 20. Map of maximum principal stresses for the POT-12 series.

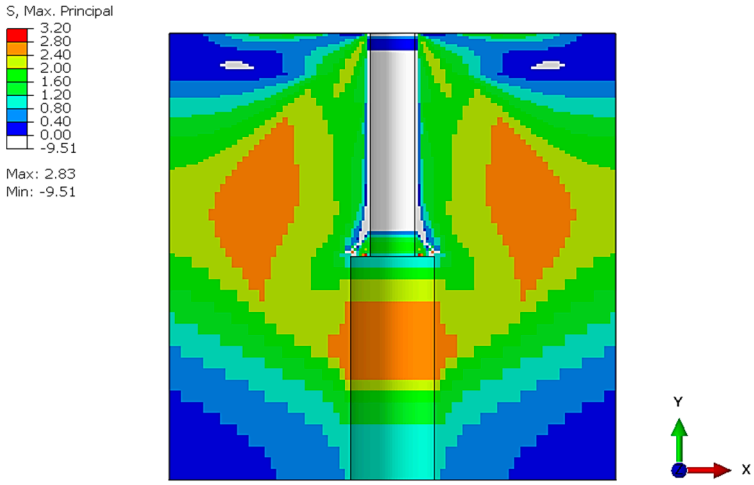

Figure 21. Map of maximum principal stresses for the POT-16 series.

During the pull-out tests, the POT-16 series specimens were damaged by splitting, which is evident from the curve shown in Figure 14. This means that the vertical component of the bond force, causing radial compressive stresses in the cracked bar cover and circumferential tensile stresses in the uncracked bar cover [52], was dominant due to insufficient bar confinement in the concrete. This should lead to exceeding the concrete tensile strength and splitting the concrete. From the map of maximum principal stresses (maximum tensile stresses, Figure 21), the maximum tensile stress occurring in the specimen had a value of 2.83 MPa, and at the edge of the block, about 2.40 MPa. Equal parameter values for the concrete material model were used for the numerical analysis of the POT. Table 15 shows the mean concrete tensile strengths for each series of pull-out test.

Table 15. Mean value of concrete tensile strength (f_{ctm}) according to pull-out test series (in MPa).

POT-10 [MPa]	POT-12 [MPa]	POT-16 [MPa]
3.33	3.22	2.71

As can be seen, the mean value of f_{ctm} was the lowest for the POT-16 series. Therefore, the FEM simulation of the POT-16 series was carried out for the modified concrete tensile strength equal to 2.71 MPa. Figure 22 presents the result of this simulation, namely the map of the maximum principal stresses in the concrete block corresponding to the maximum bond stress.

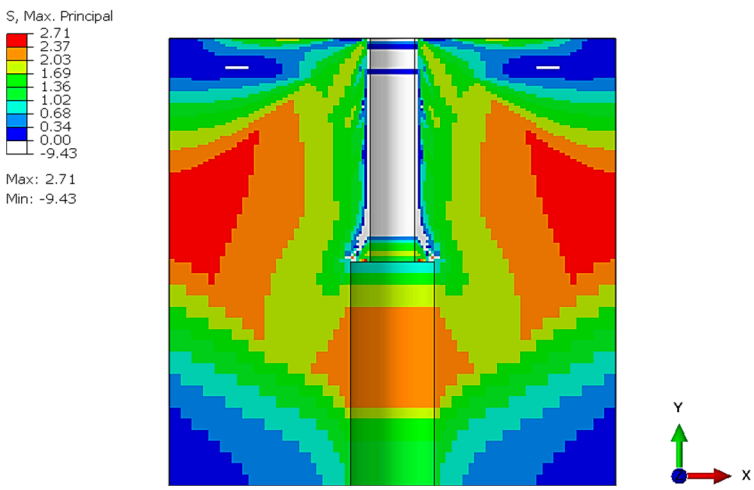

Figure 22. Map of maximum principal stresses for POT-16 series for modified concrete material model.

From Figure 22, it can be seen that the introduced modification of the concrete material model affected the tensile stresses in the concrete. This view of tensile stresses prompts the conclusion that the concrete block of the specimen would be damaged by splitting failure, which is what happened in the experimental study.

5. Conclusions

Based on the conducted analysis, the following conclusions can be drawn:

- The diameter of the bar is a quantity that determines the dimensions of the concrete block and bond length in the pull-out test. It affects the bond behavior in the test, that is, the course of the local bond stress–slip relationship, as well as the pull-out force, which increases as the bar diameter increases.
- For test pieces in which the bond length does not exceed five times the bar diameter, the bond stress is treated as a pull-out force uniformly distributed on the lateral surface of the bar, cooperating with the concrete. Thus, the maximum stress τ_b has similar values for different bar diameters and for the same type of bond failure. This is an important conclusion in the context of the division of bars into groups in terms of bar diameter, which was presented in the standard [18].
- If a concrete block of the same size is used, the bar confinement by the concrete cover depends on the diameter d_b. The conducted tests confirmed the notation in MC2010 [4] regarding the ratio of the bar cover thickness to its diameter. Specimens from the POT-10 and POT-12 series, in which the condition $c/d_b \geq 5$ was met, were damaged by pull-out.
- The Contact Cohesive Behavior (CCB) method effectively reproduces the effect of bond at the concrete–bar interface in the pull-out test. The use of this method in FEA simulations performed in ABAQUS allowed for the obtainment of $\tau_b(s)$ curves consistent with the experimental results.
- The numerical simulations performed showed how important it is to properly define material models that correctly reflect the operation of the POT specimen. If the material models are properly defined, it is possible to observe and analyze results that are unknown during experiments (e.g., stress analysis in concrete).
- The correct determination of parameters specifying bond behavior, such as stiffness and damaged initiation and evolution, is crucial for the simulation of concrete–bar interface performance. In the presented numerical analysis of the POT, the local bond stress–slip relationship contained in MC2010 [4] was used. The characteristic points were determined using representative curves obtained from experiments. This solution was chosen because the $\tau_b(s)$ curves according to MC2010 [4] correctly reflected the trend of the experimental curves, while the characteristic points of the graph, which are mainly determined by the maximum bond stress, were characterized by significant discrepancies from the POT results, as shown by the parametric analysis performed. This conclusion indicates that the topic of research on improving models of the local bond stress–slip relationship is still an open issue, which will form the basis for further research by the authors of this paper.

Author Contributions: Conceptualization, M.B. and M.N.; data curation, M.B. and M.N.; formal analysis, M.B.; funding acquisition, M.B. and M.N.; investigation, M.B.; methodology, M.B.; project administration, M.B. and M.N.; resources, M.B. and M.N.; software, M.B.; supervision, M.N.; validation, M.B. and M.N.; visualization, M.B.; writing—original draft preparation, M.B.; writing—review and editing, M.B. and M.N. All authors have read and agreed to the published version of the manuscript.

Funding: This research received no external funding.

Institutional Review Board Statement: Not applicable.

Informed Consent Statement: Not applicable.

Data Availability Statement: Not applicable.

Acknowledgments: The authors of this paper would like to thank The Centre of Informatics Tricity Academic Supercomputer & Network for the possibility of using high-power computers for numerical calculations.

Conflicts of Interest: The authors declare no conflict of interest.

References

1. Xing, G.; Zhou, C.; Wu, T.; Liu, B. Experimental Study on Bond Behavior between Plain Reinforcing Bars and Concrete. *Adv. Mater. Sci. Eng.* **2015**, *2015*, 604280. [CrossRef]
2. Rehm, G. Über die Grundlagen des Verbundes zwischen Stahl und Beton, Deutscher Ausschuß für Stahlbeton 1961. p. 138. Available online: https://www.amazon.co.uk/Grundlagen-Verbundes-zwischen-Stahl-Beton/dp/B0000BMOQG (accessed on 5 May 2022).
3. International Federation for Structural Concrete. *fib Bulletin 10. Bond of Reinforcement in Concrete (State-of-Art Report)*; International Federation for Structural Concrete: Lausanne, Switzerland, 2000.
4. CEB. *CEB-FIP Model Code 2010*; CEB: Lausanne, Switzerland, 2010.
5. Watstein, D. Bond stress in concrete pull-out specimens. *J. Proc.* **1941**, *38*, 37–52.
6. Watstein, D. Distribution of Bond Stress in Concrete Pull-Out Specimens. *J. Proc.* **1947**, *43*, 1041–1052.
7. Tekle, B.H.; Khennane, A.; Kayali, O. Bond Properties of Sand-Coated GFRP Bars with Fly Ash–Based Geopolymer Concrete. *J. Compos. Constr.* **2016**, *20*, 04016025. [CrossRef]
8. Nadir, Y.; Sujatha, A. Bond strength determination between coconut shell aggregate concrete and steel reinforcement by pull-out test. *Asian J. Civ. Eng.* **2018**, *19*, 713–723. [CrossRef]
9. Wei, W.; Liu, F.; Xiong, Z.; Lu, Z.; Li, L. Bond performance between fibre-reinforced polymer bars and concrete under pull-out tests. *Constr. Build. Mater.* **2019**, *227*, 116803. [CrossRef]
10. Li, X.; Zhang, J.; Liu, J.; Cao, W. Bond Behavior of Spiral Ribbed Ultra-high Strength Steel Rebar Embedded in Plain and Steel Fiber Reinforced High-Strength Concrete. *KSCE J. Civ. Eng.* **2019**, *23*, 4417–4430. [CrossRef]
11. Sadeghi, N.; Sharma, A. Pull-Out Test for Studying Bond Strength in Corrosion Affected Reinforced Concrete Structures—A Review. *Otto-Graf-J.* **2019**, *18*, 259–272.
12. Lei, W.; Jin, Y.; Hailong, X.; Lei, F. Experimental study of a pull-out test of corroded steel and concrete using the acoustic emission monitoring method. *Constr. Build. Mater.* **2016**, *122*, 163–170.
13. Solyom, S.; Di Benedetti, M.; Guadagnini, M.; Balazs, G.L. Effect of temperature on the bond behaviour of GFRP bars in concrete. *Compos. B Eng.* **2020**, *183*, 107602. [CrossRef]
14. Deshpande, A.A.; Kumar, D.; Ranade, R. Temperature effects on the bond behavior between deformed steel reinforcing bars and hybrid fiber-reinforced strain-hardening cementitious composite. *Constr. Build. Mater.* **2020**, *233*, 117337. [CrossRef]
15. Pędziwiatr, J. *Basics of Bond Between Steel and Concrete in Reinforced Concrete Structures*; Publishing House of Wrocław University of Technology: Wrocław, Poland, 2007. (In Polish)
16. International Federation for Structural Concrete. *fib Bulletin 72. Bond and Anchorage of Embedded Reinforcement: Background to the fib Model Code for Concrete Structures 2010*; International Federation for Structural Concrete: Lausanne, Switzerland, 2014.
17. *EN 1992-1-1*; Eurocode 2—Design of Concrete Structures: Part 1-1: General Rules and Rules for Buildings. European Committee for Standardization: Brussels, Belgium, 2008.
18. *EN 10080*; Steel for the Reinforcement of Concrete. European Committee for Standardization: Brussels, Belgium, 2007.
19. Rilem, T.C. *RILEM Recommendations for the Testing and Use of Construction Materials, RC 6 Bond Test for Reinforcement Steel. Pull-Out Test, 1983*; E&FN SPON: London, UK, 1994.
20. Eligenhausen, R.; Bertero, V.V.; Popov, E.V. *Local Bond Stress-Slip Relationships of Deformed Bars under Generalized Excitations: Tests and Analytical Model*; Technical Report UCB/EERC-83; Earthquake Engineering Research Center: Berkeley, CA, USA, 1983.
21. Araujo, D.L.; Danin, A.R.; Melo, M.B.; Rodrigues, P.F. Influence of steel fibres on the reinforcement bond of straight steel bars. *Ibracon Struct. Mater. J.* **2013**, *6*, 307–338.
22. Hameed, R.; Turatsinze, A.; Duprat, F.; Sellier, A. Bond stress-slip Behaviour of Steel Reinforcing Bar Embedded in Hybrid Fiber-reinforced Concrete. *KSCE J. Civ. Eng.* **2013**, *17*, 1700–1707. [CrossRef]
23. Guizani, L.; Chaallal, O.; Mousavi, S.S. Local bond stress-slip model for R/C joints and anchorages with moderate confinement. *Can. J. Civ. Eng.* **2017**, *44*, 201–211. [CrossRef]
24. Gambarova, P.G.; Rosati, G.P. Bond and splitting in reinforced concrete: Test results on bar pull-out. *Mater. Struct.* **1996**, *29*, 267–276. [CrossRef]
25. Tang, C.W.; Cheng, C.K. Modeling Local Bond Stress-Slip Relationships of Reinforcing Bars Embedded in Concrete with Different Strengths. *Materials* **2020**, *13*, 3701. [CrossRef]
26. Carvalho, E.P.; Ferreira, E.G.; da Cunha, J.C.; Rodrigues, C.S.; Maia, N.S. Experimental Investigation of Steel-Concrete Bond for Thin Reinforcing Bars. *Lat. Am. J. Solids Struct.* **2017**, *14*, 1932–1951. [CrossRef]
27. Murcia-Delso, J.; Stavridis, A.; Shing, B. Modeling the Bond-Slip Behavior of Confined Large-Diameter Reinforcing Bars. In Proceedings of the ECCOMAS Thematic Conference—COMPDYN 2011: 3rd International Conference on Computational Methods in Structural Dynamics and Earthquake Engineering, Corfu, Greece, 25–28 May 2011.

28. Issa, C.A.; Masri, O. Numerical Simulation of the Bond Behavior between Concrete and Steel Reinforcing Bars in Specialty Concrete. *Int. J. Civ. Environ. Eng.* **2015**, *9*, 767–774.
29. Li, D.; Gravina, R.; Zhuge, Y.; Mills, J.E. Bond behaviour of steel-reinforcing bars in Crumb Rubber Concrete (CRC). *Aust. J. Civ. Eng.* **2020**, *18*, 2–17. [CrossRef]
30. Pereira, H.; Cunha, V.; Sena-Cruz, J. Numerical simulation of galvanized rebars pullout. *Frat. Integrita Strutt.* **2015**, *31*, 54–66. [CrossRef]
31. Hu, Z.; Shah, Y.I.; Yao, P. Experimental and Numerical Study on Interface Bond Strength and Anchorage Performance of Steel Bars within Prefabricated Concrete. *Materials* **2021**, *14*, 3713. [CrossRef] [PubMed]
32. Rolland, A.; Argoul, P.; Benzarti, K.; Quiertant, M.; Chataigner, S.; Khadour, A. Analytical and numerical modeling of the bond behavior between FRP reinforcing bars and concrete. *Constr. Build. Mater.* **2020**, *231*, 117160. [CrossRef]
33. Bravo, M.; Duarte, A.P.C.; de Brito, J.; Evangelista, L. Tests and Simulation of the Bond-Slip between Steel and Concrete with Recycled Aggregates from CDW. *Buildings* **2021**, *11*, 40. [CrossRef]
34. Burdziński, M.; Niedostatkiewicz, M.; Ziółkowski, P. Tests of bond between concrete and steel bars—literature background and program of own research. *Bud. Archit.* **2020**, *19*, 5–19. [CrossRef]
35. *EN 206*; Concrete. Specification, Performance, production and conformity. European Committee for Standardization: Brussels, Belgium, 2021.
36. *EN 197-1*; Cement—Part 1: Composition, specifications and conformity criteria for common cements. European Committee for Standardization: Brussels, Belgium, 2012.
37. *EN 12390-3*; Testing Hardened Concrete. Compressive Strength of Test Specimens. European Committee for Standardization: Brussels, Belgium, 2019.
38. *EN 12390-6*; Testing Hardened Concrete. Tensile Splitting Strength of Test Specimens. European Committee for Standardization: Brussels, Belgium, 2011.
39. *EN 12390-13*; Testing Hardened Concrete. Determination of Secant Modulus of Elasticity in Compression. European Committee for Standardization: Brussels, Belgium, 2014.
40. *EN 12350-2*; Testing fresh Concrete—Part 2: Slump Test. European Committee for Standardization: Brussels, Belgium, 2019.
41. *PN-H-93220:2018-02*; Steel for Concrete Reinforcement—Weldable Reinforcing Steel B500SP. Polish Committee for Standardization: Warsaw, Poland, 2018.
42. *EN ISO 15630-1*; Steel for the Reinforcement and Prestressing of Concrete—Test Methods—Part 1: Reinforcing Bars, Rods and Wire. European Committee for Standardization: Brussels, Belgium, 2019.
43. Abaqus 2020. User Assistance (Online Documentation). SIMULIA. Available online: http://194.167.201.93/English/DSSIMULIA_Established.htm (accessed on 5 May 2022).
44. Keuser, M.; Keep, B.; Mehlhorn, G.; Rostásy, F. Nonlinear static analysis of end-fittings for GFRP-prestressing rods. *Comput. Struct.* **1983**, *17*, 719–730. [CrossRef]
45. Baena, M.; Torres, L.; Turon, A.; Barris, C. Experimental study of bond behaviour between concrete and FRP bars using a pull-out test. *Compos. B Eng.* **2009**, *40*, 784–797. [CrossRef]
46. Liang, R.; Huang, Y.; Xu, Z. Experimental and Analytical Investigation of Bond Behavior of Deformed Steel Bar and Ultra-High Performance Concrete. *Buildings* **2022**, *12*, 460. [CrossRef]
47. Harajli, M.H.; Hout, M.; Jalkh, W. Local bond stress-slip behaviour of reinforcing bars embedded in plain and fiber concrete. *ACI Mater. J.* **1995**, *92*, 343–353.
48. *AS3600*; Australian Standard for Concrete Structures. Australian Standard for Concrete Structures: North Sydney, NSW, Australia, 1994.
49. Orangun, C.O.; Jirsa, I.O.; Breen, J.E. A Reevaluation of Test Data on Development Length and Splices. *ACI J.* **1977**, *74*, 114–122.
50. Darwin, D.; McCabe, S.L.; Idun, E.K.; Schoenekase, S.P. Development Length Criteria: Bars Not Confined by Transverse Reinforcement. *ACI Struct. J.* **1992**, *89*, 709–720.
51. Huang, Z.; Engström, B.; Magnusson, J. *Experimental Investigation of the Bond and Anchorage Behaviour of Deformed Bars in High Strength Concrete (Report 95:4)*; Chalmers University of Technology: Gothenburg, Sweden, 1996.
52. Tastani, S.P.; Pantazopoulou, S.J. Direct Tension Pullout Bond Test: Experimental Results. *J. Struct. Eng.* **2010**, *136*, 731–743. [CrossRef]